ORIGINAL ARTICLE

Deformation behavior in tube bending: a comparative study of compression bending and rotary draw bending

Sigmund A. Tronvoll[1] · Jun Ma[1] · Torgeir Welo[1]

Abstract

As the first study in the field regarding CB, this paper investigates the implications of interchanging between RDB and CB through manufacturing bends with various angles and investigates the difference between the two methods in form of springback, cross section compression and widening, cross section shape and wall thinning/thickening. The experiments conducted consists of aluminum alloy 6060-T4 round tubes of 60 mm diameter and 3 mm wall thickness, bent around 222 mm radius tooling with various bend angles. In this case, we have found that CB is capable of manufacturing bends with quality near those manufactured by RDB with less springback, however with a dimensional penalty regarding increased deformation of the cross section.

Keywords Compression bending · Rotary draw bending · Metal forming · Aluminum profiles

1 Introduction

Bending is an essential process for forming tubular parts. As noted by both Kervick and Springborn [1], and more recently, Miller [2], manufacturers have largely adopted *rotary draw bending* (RDB) as the main process for automated manufacturing of high-precision tube bends with tight radii. For increasing the flexibility of the manufacturing equipment, many companies use multi-tool-stack tube bending machines, commonly equipped with a stack for *three roller push bending* (TRPB). These combined TRPB-RDB tools have also been addressed in multiple research studies, as in the research by Ghiotti et al.[3] assessing springback in TRPB, and in a study regarding automatic wrinkle detection for TRPB by Simonetto et al. [4]. The TRPB stack increases the capability of the equipment because it is able to create larger curves or spline-geometries. The *forming roller* on such TRPB stacks is often placed on the same arm as the clamp die for RDB, thus moving tangentially to the bend die. By moving the forming roller, while keeping the tube stationary, the machine is also able to perform *compression bending* (CB), in addition to its main application of performing TRPB and RDB, as illustrated in Fig. 1.

As RDB has been the most popular process for tight-radius bends in industrial manufacturing systems since the late 1960s, CB has attracted very little academic attention in capability studies. To our knowledge, no studies in the open literature give data showing if the capabilities and performance of CB are significantly different from RDB. Therefore, we argue that since these tooling setups are readily available in many workshops, there is a large upside in researching the implications of using CB as an alternative to RDB, as it can provide some benefits:

- CB produces lower scrap rates, as there is no end clamp as needed for RDB,
- CB enables the possibility to make a spline that translates into a small radius bend due to the lack of an end clamp, and
- the CB process can act as redundancy in case of RDB tooling breakdown on a dual-stack setup.

The only downside mentioned in prior literature, in e.g., textbooks by Kervick and Springborn [1] and Miller [2], is less controllable deformation characteristics, and hence more severe geometric distortions. In addition, mandrel systems are less convenient for CB, as it would require a so-called flexible mandrel system equivalent to the bend length. Because of

✉ Sigmund A. Tronvoll
sigmund.tronvoll@ntnu.no

[1] Department of Mechanical and Industrial Engineering, NTNU - Norwegian University of Science and Technology, Trondheim, Norway

Fig. 1 Schematic overview of compression bending using rollers (right) and rotary draw bending (left). Blue arrows indicate the movement of parts during bending
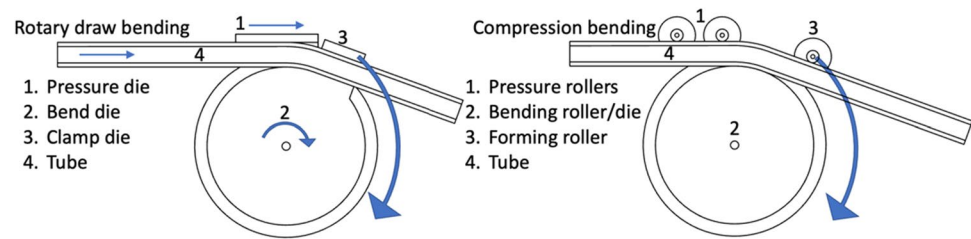
these mandrel limitations, and that the force transfer between the tools and the tube is through the roller's curved surfaces with little contact area, the process capability is expected to be inferior to that of RDB. For RDB, the interaction between pressure die, mandrel and wiper die is crucial for achieving high quality bends with high D/t ratios (tube diameter to thickness ratio) and low R/D ratios (bend radius to tube diameter ratio) as researched by He et al. [5] and He and Lin [6] among others, as these impose constraints on the mechanisms leading to wrinkling.

To be able to shift between RDB and CB, a clear overview of the potential implications of using CB must be assessed. This paper will therefore investigate various dimensional characteristics of tubes bent by CB and compare these with those of similar parts made by RDB. The investigation will be conducted through experiments using Ø60×3 mm tubes of aluminum alloy 6060-T4 bent around a bend die with a radius of 222 mm, at various bend angles. The main research questions are:

- How do the two methods (RDB and CB) differ in terms of capabilities related to:
  - springback angle,
  - cross-sectional distortion,
  - wall thinning/thickening?
- Could mandrel-less RDB be substituted by CB—and what would be the conditional parameters?

After a brief introduction to the background theory, the paper will present the experimental setups. Then, it presents the results of the physical experiments conducted to compare CB and RDB, quantifying how the two processes perform in terms of cross-sectional deformation, springback, and wall thickening/thinning for various angles. A numerical analysis of the two processes will be used to support the argumentation in the discussion. The results are then evaluated based on what they reveal in terms of interchangeability between RDB and CB. Finally, the conclusion is drawn in Section 4.

2 Background and methodology

2.1 Background

As tube bending generally requires severe non-linear plastic deformation of multiple non-constrained surfaces, dimensional defects are unavoidable. Common dimensional defects for tube bending are:

- cross-sectional deformation ("ovalization," sagging, compression, widening or other),
- wall thinning and thickening on the extrados and intrados, respectively,
- elastic springback, reducing the nominal bend angle and increasing the realized bend radius upon unloading,
- discrete detrimental and visual defects (wrinkling, fracture, galling, etc.).

These and their variability will be the main aspects of investigation throughout this paper.

The cross-sectional deformation of round tubes has been investigated experimentally and numerically in many studies. One of the first major contributions to the understanding of deformation behavior during tube bending was the description of cross-section flattening by Brazier and Southwell [7], and hence called the Brazier effect. Hill [8] assessed the governing mechanisms for cross-section distortions in his general theory of sheet bending. Pan and Stelson [9] investigated the influence of wall thickness and finite bend length on the deformation characteristics, and created a numerical approach for this problem. Paulsen and Welo [10] created an analytical framework taking into account the bend radius and the wall thickness-tube diameter ratio. Some refer to the local deformation characteristics of round tubes as ovalization. However, theoretically, ovalization strictly applies only to pure bending problems at large radii, which is rarely the case. For both CB and RDB, the tooling creates significant

contact forces and constraints making the pure bending simplification questionable for useful assessments. Moreover, as the *profile depth-to-moment arm length* ratio is rather high, shear deformations would often play a significant role for local deformations. Both the early numerical approach by Pan and Stelson [9] and numerical studies by Safdarian [11] show that the RDB process generates deformations that are highly unsymmetric across the neutral layer of the cross section, approaching a D-shape rather than oval cross-section, with flattened extrados and rounded intrados. These deformation characteristics are expected to also be inherent to the CB process.

Tube wall thinning and thickening are consequences of the deviatoric nature of plastic deformation, making the wall thickness increase if the longitudinal plastic bending strain is compressive (as on the intrados), and decrease in areas with tensile average longitudinal strain (as on the extrados). This effect is well known and included in the model by Pan and Stelson [9], and its dependence on bend radius to tube diameter is shown in a study by Li et al. [12]. As there is an expected difference in longitudinal plastic bending strain for CB compared to RDB due to mechanical loading differences of the two processes, this is expected to give some variation in the resulting wall thicknesses.

Elastic springback is the deformation caused by release of elastic strain energy in the system. It is therefore a function of both the strain field, the yield behavior of the material and elastic properties of the material. Due to the expected difference in strain field between RDB and CB, elastic springback is also expected to vary between the two.

Discrete defects are a broad class of deformations, including both detrimental and visual ones, with the most common modes being wrinkling, fracture and galling. Moreover, as demonstrated by Yang et al. [13], many of them are intercoupled or coupled with the previously mentioned defects, and also sensitive to friction and tool interface conditions. One of the more common defects, wrinkling, is caused by large compressive stresses, combined with low instantaneous inelastic stiffness of cross-sectional members causing low buckling resistance. Onset of wrinkling is therefore a problem often encountered in thin-walled tubes or profiles with plane surfaces (e.g., rectangular hollow profiles). In this study we have chosen to use a tube diameter-to-thickness ratio of 20, which positions the case outside the class of typical thin-walled tubes. Therefore, wrinkling is not expected to be a major concern, even when bending without a mandrel. Galling has a more unclear interface mechanism as noted by Dohda et al. [14], but according to Kim et al. [15] this is often caused by excessive contact and friction forces over time, due to inadequate tooling or process setup in combination with a high tool-workpiece material similarity. Defects resulting in fracture are a result

of forming to such an extent that strain exceeds the limits of the applied stress state. This may be only due to reaching the process limits of the profile height and bend ratio, or it may be in combination with other defects such as galling or wrinkling.

RDB is a well-established and frequently investigated method for tube bending. It is the preferred production method for creating bends on tubes and more complex profiles with relatively small tube-to-bend-diameter. RDB is thus a practical benchmark for evaluating CB, known for its capability of producing bends with good dimensional results. The core process of rotary draw bending could be described by (1) clamping the tube end to the bend die, allowing for moment transfer from the tooling to the tube. and (2) counteracting the bending moment by using a moveable pressure die for minimizing the traction between tube and the pressure die. On some machines, the speed of this pressure die can be controlled, and tuned to minimize surface defects or optimizing the bend geometry. One of the drawbacks of RDB, however, is the need for providing a certain straight tube portion available at the end of the bend for the clamp die to be able to hold the tube firmly. For product configurations requiring no such straight section, this introduces process scrap that would need to be removed in a separate operation after bending (end cuts) and ultimately recycled. In addition, the required straight portion makes it impossible to position two bends right after another without making specialized clamp dies. For thin-walled tubing and/or very small bending radii, additional tools, such as internal mandrels and intrados wiper dies, are often used to reduce cross-sectional deformation. While being essential for bending thin-walled tubing, as displayed by Heng et al. [16], bending without mandrel or wiper die is being successfully performed for medium and thick-walled tubes, as displayed by Ma et al. [17]. Bending without a mandrel has its economic upsides, as this is a relatively expensive tool, and would need to be fitted to the internal dimension of each profile. The complex contact forces generated by the mandrel, which depend on the mandrel design and insertion length, create numerous additional process parameters and more uncertainty in numerical results. The experiments in this study are therefore run without a mandrel to increase the general applicability of the findings. A wiper die has been deemed unnecessary due to a modest diameter-to-thickness ratio, and to reduce the number of variables in the experiment.

Although CB is a commonly used method for manual bending operations, it has not attracted much interest in the academic literature. This is true for both classical CB and roller-based CB, as described in this paper. In contrast to *roller-based CB*, *classical CB* utilizes a setup where the stationary rollers are replaced with a stationary clamp, and the forming roller is replaced with a sliding clamp. Although common for manual bending of small radius pipes with hand tools, this method is relatively rarely utilized in industrial

automated bending because of the claim of reduced performance in comparison to RDB. In the continuation, the abbreviation CB will be used for denoting roller-based CB only, unless stated otherwise. We have only identified three sources that mention roller-based CB: Kervick and Springborn [1], Miller [2] and Tekkaya and Chatti [18]. However, these sources display a bending operation with a clamp filling the same function as pressure rollers and collet provided in three roller push bending, keeping the tube end in a stationary position during bending.

Kervick and Springborn [1] and Miller [2] describe CB as less capable of controlling the material flow as compared with RDB. Moreover, the latter describes that it requires a relatively high bend radius to tube height ratio (preferably above 4). Tekkaya and Chatti [18] mention roller based CB as an example of what they call "form closed bending contour–rotary tool motion" tube bending process, alongside the similar process of *wiper-bending, stretch bending* and RDB. They state no specific process-related qualities, other than being less flexible than the "kinematically defined bending contour processes," e.g., TRPB which is capable of generating a wide range of curvatures. There is some research covering TRPB, but although the tooling is identical, the load conditions and overall process are considered too dissimilar to be used as a background for this paper. Neither did we identify any articles investigating classical CB thoroughly. However, it is noted that this is identical to RDB with a stationary bend die, without mandrel and pressure die, and the collet disengaged upon bending. This RDB configuration has been investigated by Borchmann et al. [19] and shows a penalty in maximal strain levels by having the pressure die fixed. In their specific case of bending 40 mm diameter tubes with a 2 mm thickness manufactured in steel grade 1.4301, bent around a die with 1.875 bend-radius-to-tube-diameter, having a fixed pressure die rather than moving with the same

velocity as the tube, resulted in 42% increased maximum strain in the extrados. As some of the motivation for this paper is investigating potential upsides of using the TPRB-stack for compression bending as an alternative for RDB, we do not investigate classical CB further herein.

In addition to the bend die radius, tube diameter and thickness (R_{BD}, D_t, t_t), the most common configuration of CB using TRPB tooling has multiple additional fundamental parameters (as seen in Fig. 2): forming rollers and pressure roller rake distances (d_{FR}, d_{PR1}, and d_{PR2}) and roller diameter ($D_{FR/PR1/PR2}$).

From an analytical standpoint, roller-based CB is expected to have larger dimensional defects than RDB due to the following differences in basic mechanism involved, as illustrated in Fig. 3, including:

- Larger contact pressure between forming roller and tube than between pressure die and tube, due to large curvature of the forming roller.
- The zone where the largest plastic deformation occurs for a tube in CB (tangent point between bend die and tube) is only supported by the bend die, while for RDB the pressure die gives additional support.
- Conventional systems are unable to effectively combine a mandrel with compression bending.

As illustrated in Fig. 3, the moment-to-shear force ratio caused by the forming roller pressure in CB is likely to be higher than the one generated by the pressure die for RDB. The main reason is the distance between the tube/bend die tangent point to the contact pressure resultant is larger for the forming roller in CB, than for the pressure die in RDB. This could reduce shear deformations, and the moment-to-shear ratio could be increased further by increasing the rake distance. However, an undesirable side

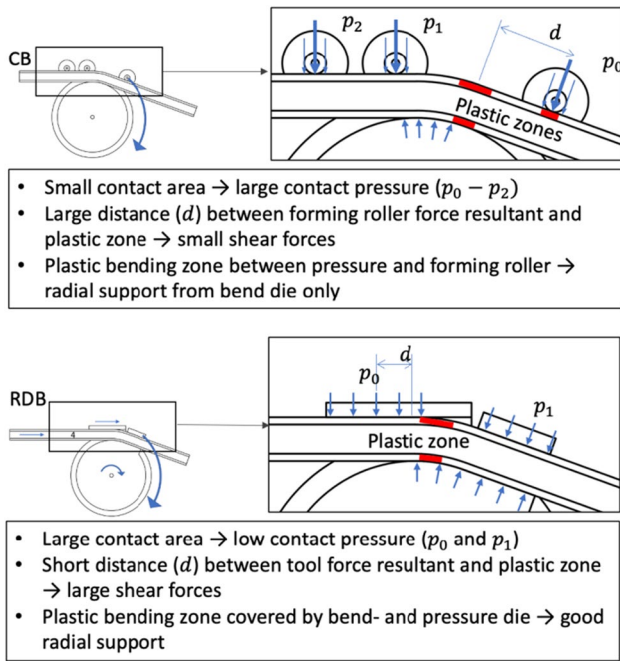**Fig. 2** Dimensional process parameters for CB tooling
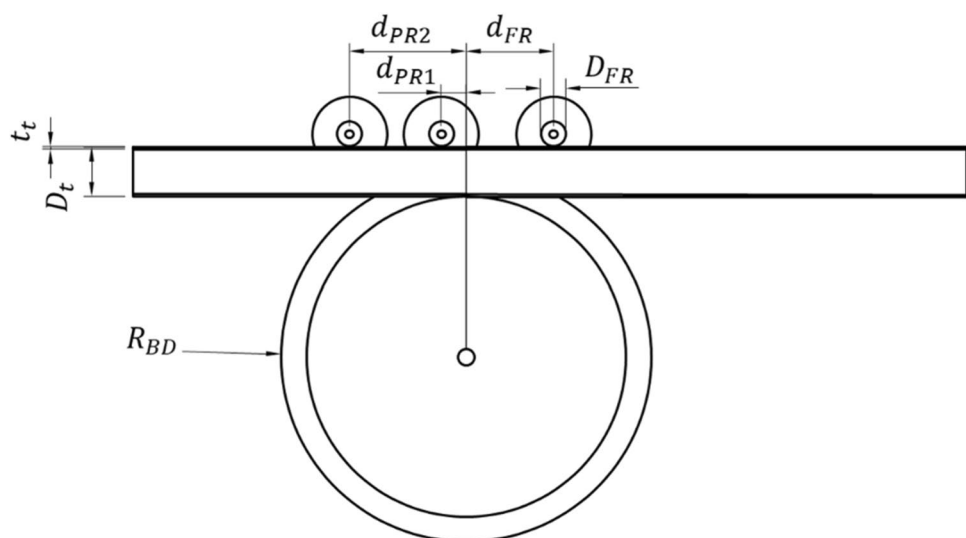
Fig. 3 Main conceptual differences in mechanisms between CB and RDB

Fig. 4 Specimen geometry

effect is that a larger rake distance would also give larger springback values owing to a larger elastic deformation zone of the bent part prior to unloading. In addition, a larger rake distance requires a longer section of tubing available on the end of the bend on which the forming roller pushes. Choosing the optimal value would therefore be a trade-off between these three considerations. The contact pressure for CB compared with RDB could be reduced by using a larger diameter forming roller. However, it would be unlikely to achieve the same low local pressure as for RDB due to the curvature of the forming roller.

Methods for improving the process in terms of radial support wiper bending by adding sideways support are proposed by Kale and Thorat [20]. This process requires groove-less bend dies and forming rollers and is thus not possible to perform on conventional TRPB tooling. This is therefore not covered in detail in this study.

2.2 Material and characterization

AA6060-T4 tubes were used as material in this study. The nominal outer diameter is 60 mm and the nominal thickness is 3 mm. The tubular materials were supplied by Hydro Extrusions, for which the nominal chemical composition could be found in the material data sheet [21], and the
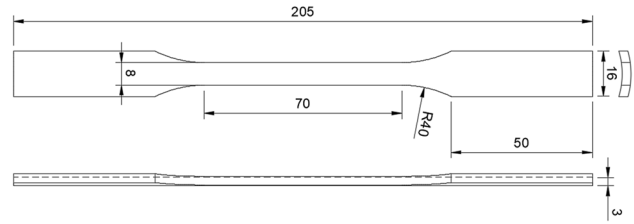
material data used for numerical investigation was obtained by a test procedure. Uniaxial tensile tests were conducted in an *Instron ElectroPuls E10000* universal test machine at a nominal strain rate of 0.04 min^{-1}, providing quasi-static conditions. Figure 4 illustrates the geometry of the "dogbone" samples cut from the as-received tubes. The gauge length and width are 70 mm and 8 mm, respectively. The ends of the cut samples were pressed planar before testing to fit in standard planar clamps. Per Saint–Venant's principle, it is assumed that the effect of non-planar samples is negligible in the plastic domain, when using relatively long specimens and applying digital image correlation (DIC) far from the clamping area for strain measurements. A camera together with the software *VIC 2D* was used to measure the deformation and analyze the strain distribution within the gauge area during testing. Two repeated tests were carried out, and the obtained stress–strain curves show high consistency, see Fig. 5a.

By analyzing the stress–strain curves, the fundamental mechanical properties of AA6060-T4 were obtained as the 0.2% offset proof stress (initial yield stress) is $\sigma_0 = 78$ MPa and the ultimate tensile strength is $\sigma_b = 160$ MPa. The Lankford coefficient was found to be $r_0 = 0.41$ averaged over a longitudinal true strain of 2% to 13%, assuming mass conservation after significant yielding ($\varepsilon_{11} + \varepsilon_{22} + \varepsilon_{33} = 0$). The value indicates high normal anisotropy and low resistance to thinning. Considering that initial imperfections and offsets typically cause test deviations in the initial slope of the elastic range of stress–strain curves, the nominal modulus of elasticity of 69 GPa is used, according to the material datasheet (Hydro Innovation and Technology, n.d.). The true stress-true strain curve of test #1 was fitted using the Voce hardening equation, as given in the following:

$$\sigma = \sigma_0 + R(1 - \exp(-C\varepsilon)) \tag{1}$$

where $\sigma_0 = 80.60$ MPa, $R = 117.99$ MPa, and $C = 15.05$ are fitted parameters.

As shown in Fig. 5b, the Voce equation could accurately capture the work-hardening curves from the experimental results.
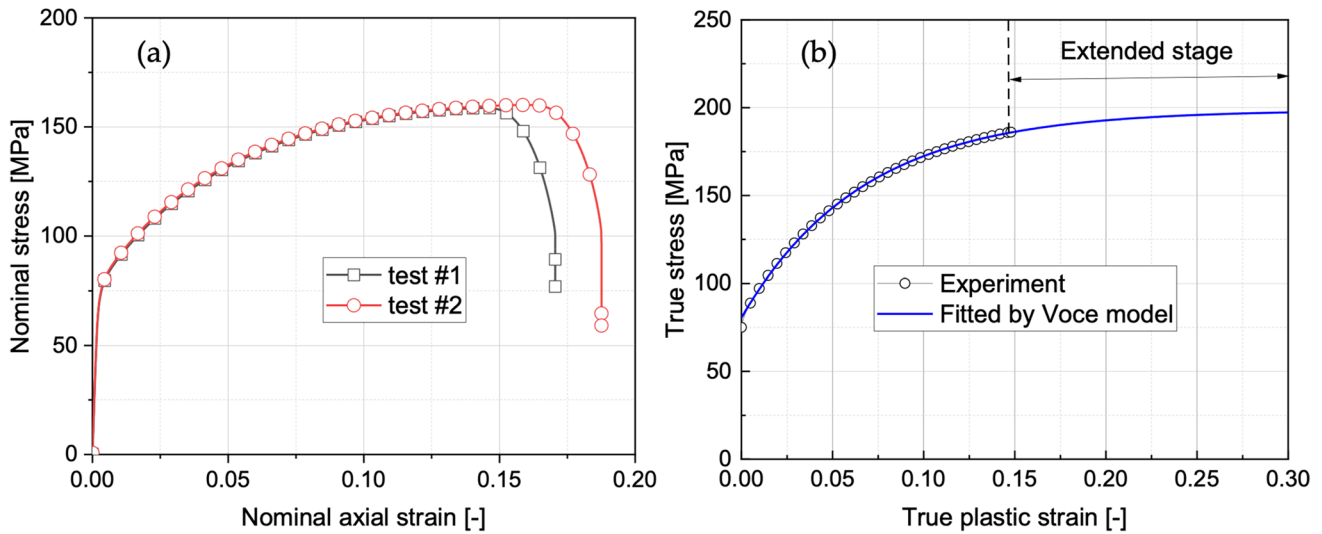
Fig. 5 Experimental stress–strain curves of AA6060-T4 tube: **a** nominal stress–strain curves; **b** true stress-true strain curves and fitted curves by Voce equation

For the finite element analysis, the Hill-48 plasticity model as described by Hill and Orowan [22], combined with the isotropic hardening law fitted by a Voce equation, was used to describe the material elastic–plastic behavior in bending processes. The Hill yield function can be written as

$$f(\sigma) = F(\sigma_{22} - \sigma_{33})^2 + G(\sigma_{33} - \sigma_{11})^2 + H(\sigma_{11} - \sigma_{22})^2$$
$$+ 2L\sigma_{23}^2 + 2M\sigma_{31}^2 + 2N\sigma_{12}^2 - \bar{\sigma}^2 = 0 \tag{2}$$

where $f(\sigma)$ is the yield function, 1, 2 and 3 refer to the principal anisotropic axes (longitudinal, transversal and through-thickness). F, G, H, L, M, and N are the anisotropic coefficients, which can be calibrated by uniaxial tension tests at relative angles of 0°, 45°, and 90°. Under the plane-stress condition, the Hill-48 model depends only on the four coefficients F, G, H, and N. Multiple methods exist to calibrate the parameters for the Hill-48 plasticity model as shown by Aretz [23], including yield stress-based, r-value based, and a combined approach using yield stress and r-values. In this study, the r-value based calibration method was used to determine the model parameters according to the relations given by Kawka [24]:

$$F = \frac{r_0}{(r_0 + 1)r_{90}} \tag{3}$$

$$G = \frac{1}{(r_0 + 1)} \tag{4}$$

$$H = \frac{r_0}{(r_0 + 1)} \tag{5}$$

$$N = \frac{(r_0 + r_{90})(2r_{45} + 1)}{(r_0 + 1)r_{90}} \tag{6}$$

Considering that tube bending is a process dominated by uniaxial tension/compression deformation, as well as the difficulty in experimental testing of mechanical properties in the hoop direction of a tube, the in-plane properties were assumed to be isotropic in this study. This was necessary to be able to establish a material model, and hence, all anisotropy values were based on the longitudinal r-value, assuming $r_0 = r_{45} = r_{90} = 0.41$. Although other models/assumptions were considered, this simplification is assumed to have negligible effect due to longitudinal plastic strain being the major plastic deformation mode, and assuming that most of the tangential plastic strain is caused by flattening or narrowing of the tangential tube curvature (wall bending). Consequently, the model parameters in the plane stress state were finally determined as follows: $F = 0.71$, $G = 0.71$, $H = 0.29$, $N = 1.29$.

2.3 Process, equipment, and production of samples

The process equipment in this study consists of a conventional dual-stack RDB/TRPB machine, *Star Technology 800 EVOBEND*, whose main specifications are listed in Table 1.

Twelve specimens of 1000 mm length each were cut from in total 4 profiles of 3000 mm length and tested in random order to spread potential variations between the profiles. All specimens have bends starting 400 mm from the end of the tube, as seen in Fig. 6.

Table 1 Process parameters

Die lubrication	SAE 40 mineral oil
Bend die radius (R_{BD})	222 mm
CB forming roller rake (d_{FR})	105 mm
CB 1st pressure roller rake (d_{PR1})	35 mm
CB 2nd pressure roller rake (d_{PR2})	145 mm
CB forming /pressure roller diameter (D_{fr})	30 mm
RDB pressure die relative velocity factor	Friction driven (measured to be 0.86)
RDB push/pull	Off (collet off while bending)
RDB pressure die length	400 mm
RDB clamp length	145 mm
Bending angles	30°, 60°, and 90°
Extrusion profile diameter (D_P)	60 mm
Extrusion profile thickness (t_P)	3 mm

2.4 Measurements

After the bending process, the resulting bend angles were measured by using a method of aligning two blocks of aluminum to the extrados over 250 mm at each end of the profile, to avoid the influence of the deformed tube section, and measuring the angle between these blocks using a *Mitutoyo 187–502* protractor.

Profile distortions were measured using a caliper for every 20 mm section on the intrados of the bend within a region 40 mm before the onset of the bend until 120 mm after the bend. Values are reported as compression/widening of the tubes radially and axially relative to the bend axis, as displayed in Fig. 7.

Then, for one 90-degree bent tube for each process, 10 mm wide segments were cut out with a band saw for the following positions: 60 mm before the start of the bend, 0°, 15°, 30°, 45°, 60°, 75°, 86.1° (average end of bend), 70 mm and 100 mm after the end of the bend. The position of the cuts was marked with a marker pen by using a paper template and a custom made marker guide as shown in Fig. 8. Assumed accuracy of position for cut is ± 6 mm, equivalent to ± 1.5°, caused by misalignment of template (approx. ± 2 mm), misalignment of marking (approx. ± 2 mm) and misalignment of cut (approx. ± 2 mm). The wall thickness of the extrados and intrados was then measured on these segments using a ball-tip digital micrometer on the middle of these segments, and hence 5 mm (1.3°) past the section position values. Due to the large tolerance for wall thickness in extrusions, the wall thickness of the extrados and intrados wall thicknesses were measured on the ends of the tube, where the average value of the tube start and end thickness for each tube makes up the nominal thickness for which the segment thicknesses are compared with.
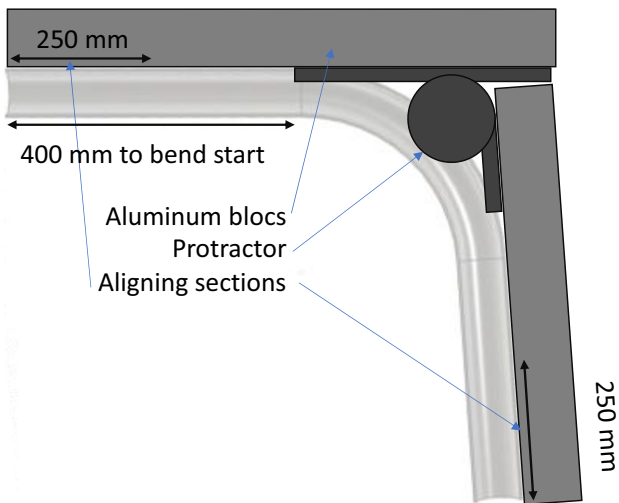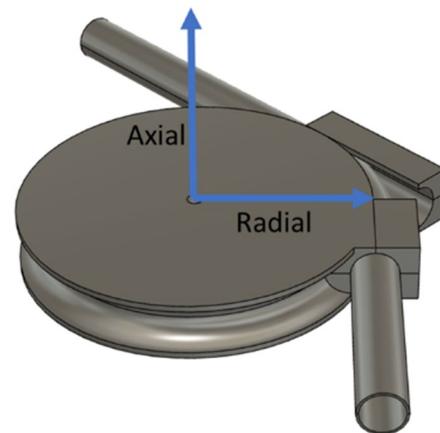

Fig. 6 Resultant bend angle measuring setup
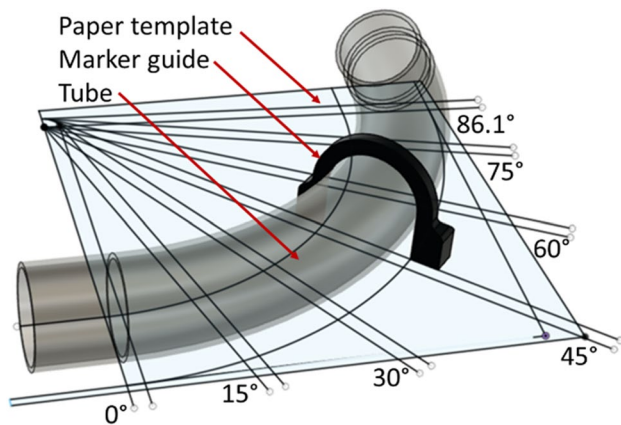

Fig. 7 Directions for measurement

Fig. 8 Segment cut marking setup

2.5 Finite element modelling

Using ABAQUS 2017, an explicit dynamic analysis was employed for both RDB and CB. Tubes were modelled using approximately 3×3 mm quadratic reduced integration shell elements (S4R) with hourglass control and 9 integration points across their thickness. Tooling was modelled as rigid, with the approximately the same element size. The models utilized symmetry, allowing for modelling only one half of the structure. A time span of 3 s was used for the bending process, with 0.5 s acceleration phase, with a mass scaling factor of 400, assuming neglectable inertia effects at this rate. A mass scaling sensitivity study was conducted for the CB simulation, as this is most prone to kinematic effects, with a mass scaling of 800, 600, 400, and 200. The maximum and minimum wall thickness change, maximum Von Mises stress at 45 degrees bend (during bending), and compression of the tube at 45 degrees position after bending was within 1% for a mass scaling of 600 to 200. Applying a scaling of 800 displayed a slightly higher stress (2.5%) but otherwise within 1%. Contact between the pressure die and pipe for RDB was modelled with a friction coefficient (m) of 0.2 (dry), between the clamp and pipe modelled with no slippage condition and the rest modelled with 0.05 friction coefficient (lubricated). Material data was determined from the previously described material tests. Assessment of accuracy was done by comparing compression of cross section and wall thinning, as this was expected to display the largest variation between CB and RDB, which is shown in Figs. 16 and 21, and elaborated on further in Sections 3.2 and 3.3.

3 Results and discussion

3.1 Springback

One sample from CB and RDB for each nominal bend angle is shown in Fig. 9. As shown in Fig. 10, RDB generates a larger average springback than CB, but seemingly with a smaller spread. However, the small sample size should be noted, with 2 samples for each process and bend angle. In addition, variability for roller-based forming methods would be highly affected by the tolerances for the tooling, especially the concentricity of the rollers and the bend die and could therefore vary significantly between tooling setups. The average difference between the processes springback range from approximately 0.2° for 30-degree samples, to 0.6° for 90-degree samples. However, the 30- and 60-degree CB samples with the largest springback have similar magnitudes to RDB samples of the same bend angle. The average sample standard deviation across the three different bend angles was 0.142° for CB, while 0.043° for RDB.

RDB shows an average springback of 2.2° for 30-degree bend angle, up to 4.2° for 90-degree bend angle. Assuming springback to be dominated by relaxation of the curvature, as compared to longitudinal contraction, this corresponds to a diametric change from the nominal 222 mm centerline radius to approximately 237 mm for 30-degree bends, down to 231.5 mm for 90-degree bends. CB display an average of 2.0° for 30-degree bend angle, up to 3.6° for 90-degree bends. The values correspond to a diametric change from the nominal 222 mm centerline radius to approximately 236 mm for 30-degree bends, down

Fig. 9 Thirty-, 60-, and 90-degree bent tubes manufactured with CB and RDB
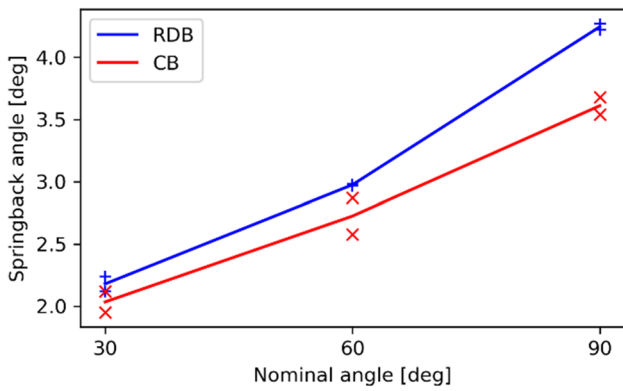
Fig. 10 Plot of springback for 30-, 60-, and 90-degree RDB and CB bends, measurements plotted as tick-marks and the average results plotted as a lines

to 230 mm for 90-degree bends. However, as there will be non-uniform compression and widening of the cross section, springback is not expected to be uniformly distributed along the bend and a variation in radius must be expected.

All these magnitudes are in the range where calibration of the process due to springback is required if, say, applying standard tolerances such as ISO 2768–1:1989, where the coarsest tolerance class for angles have limits of $\pm 1°, \pm 0.5°$, and $\pm 0.33°$ for angles with short leg lengths of 50–120 mm, 120–400 mm, and over 400 mm, respectively.

3.2 Cross-sectional distortion

As seen in Fig. 11, there is significant compression of the tubes for both processes at all angles, but with 2–3% larger compression for CB than for RDB. All tubes display a smooth inner region with no visible wrinkles or other imperfections, other than a slight dimple identified for the CB specimens at the position where the forming roller stops. This can be identified by the small jump in the compression values at approximately 80–120 mm after the stop of the bend for the CB specimens in Fig. 11, as seen in detail in Fig. 12. This dimple is caused by the high contact pressure for CB, where the entire force required to bend the tube is transferred through the curved surface of the forming roller. For RDB, however, this force is transferred over a wider area of the pressure die and thus does not result in the same denting. This is further displayed in the numerical contact pressure results in Fig. 13.

CB exhibits 2.45 times more widening on average along the bend axis (1.59 to 0.46% widening, see Fig. 11), reflecting a lack of extrados and sideways support as compared to RDB. As for the deviations in the radial direction, there are some clear anomalies at approximately the end position of the forming rollers of the CB specimens, where the tube is slightly compressed in the direction along the bend axis.

Figure 14 displays the von Mises stress during bending, where the region of the highest stress for CB is significantly longer when compared to RDB. For CB this region extends
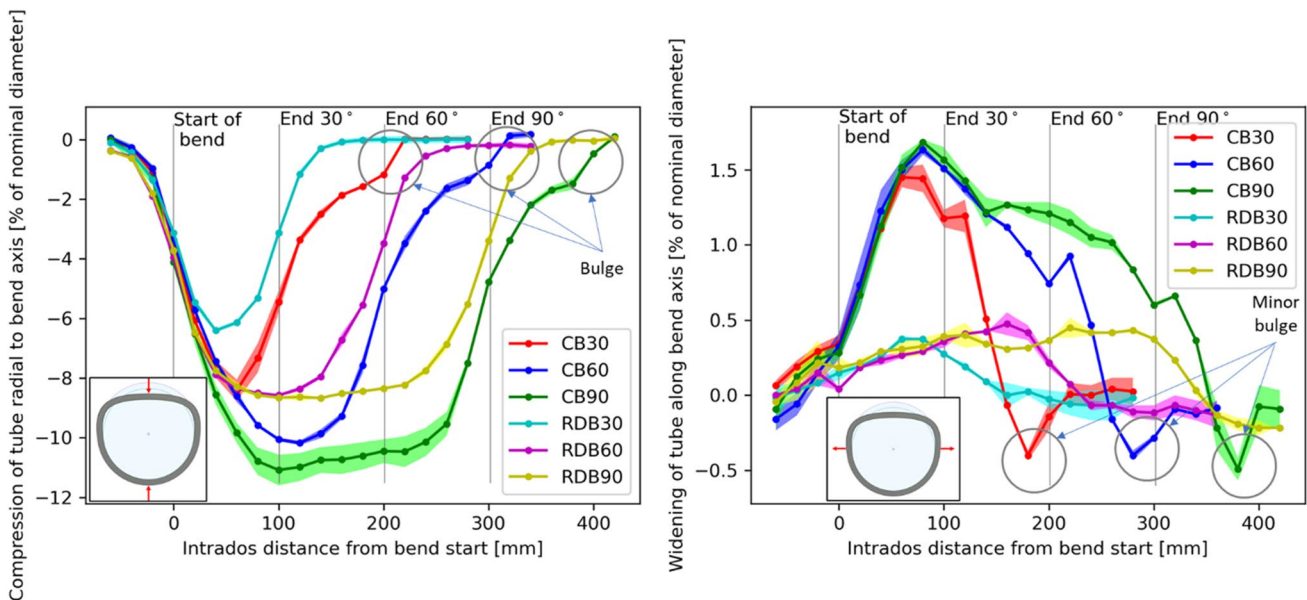

Fig. 11 Tube compression radial (flattening) to bend axis and widening along bend axis for each process/angle. Opaque zone indicates spread for the two samples per process/angle
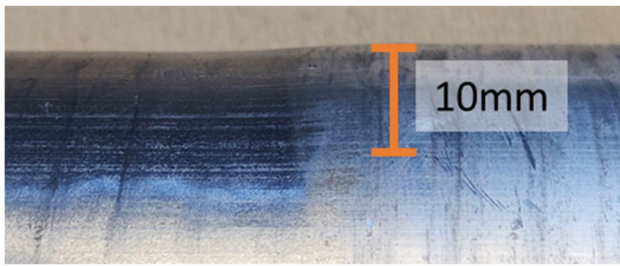
Fig. 12 Close-up of bulge at stop position of forming roller for 90-degree CB-specimen with scale bar

Fig. 14 von Mises stress in MPa of CB (upper tube) and RDB (lower tube) at 45 degrees during bending, showing that the zone of largest stress for RDB starts at the tangent point between the tube and pressure die, and extends a bit forward, while for CB is located between the forming roller and the first stationary roller. Dotted line marks identical position

from the forming roller and past the tangent point of the bend die, where the tube is only supported radially by the bend die. In RDB, this region with large von Mises stress starts approximately at the tangent point between the pressure die and the tube, where there is full radial support, and extends some distance forward from this point where the support declines gradually as the bend die and pressure die split paths. Figure 15 shows the strain derivative-to-bending angle ratio, indicating where the yielding progresses during the forming operation. As earlier explained in Fig. 3, these results show that the geometry indeed yields in the region between the bend die and pressure die for RDB. It is noted that this is a considerably more geometrically constrained region than the position of yielding for CB, which is between forming roller and bend die. In addition, significant yielding underneath the forming roller takes place.

For the 90-degree bends specifically, plots of the deviation from the nominal dimensions of the tube in the radial and axial directions relative to the bend axis are shown in Figs. 16 and 17, respectively. Images of the cross-sectional shape of the cut-out segments are shown in Fig. 18.

Cross-sectional compression results from FEA are also included in Fig. 16 for comparison. As a note on FEA-accuracy, the FEA display the same trend in the difference between RBD and CB regarding compression of the tube, showing about 1.5 mm larger compression for CB. However, both numerical results for RDB and CB display about 0.5–1 mm less compression than observed in the experiments. This discrepancy was found to be independent from mesh refinement (30% reduction in mesh size) and mass scaling refinement (50% reduction in mass scaling). As the results show a similar trend, we expect the numerical results to sufficiently replicate the difference between the methods in terms of stresses and strains, while the magnitude of these stresses and strains will differ some from the physical tests. This discrepancy between numerical and experimental results is in the same range as in the work

Fig. 13 Contact pressure on the tube exterior of RDB (lower) and CB (upper) at 45 degrees during bending, showing increased contact pressure for CB, both at the roller contact points, intrados, and along the side of the tubes where the bend die ends. Logarithmic scale
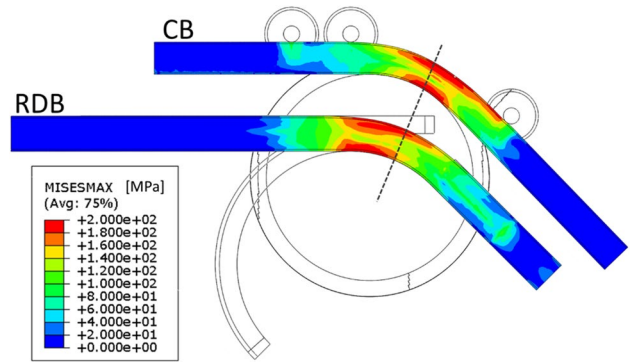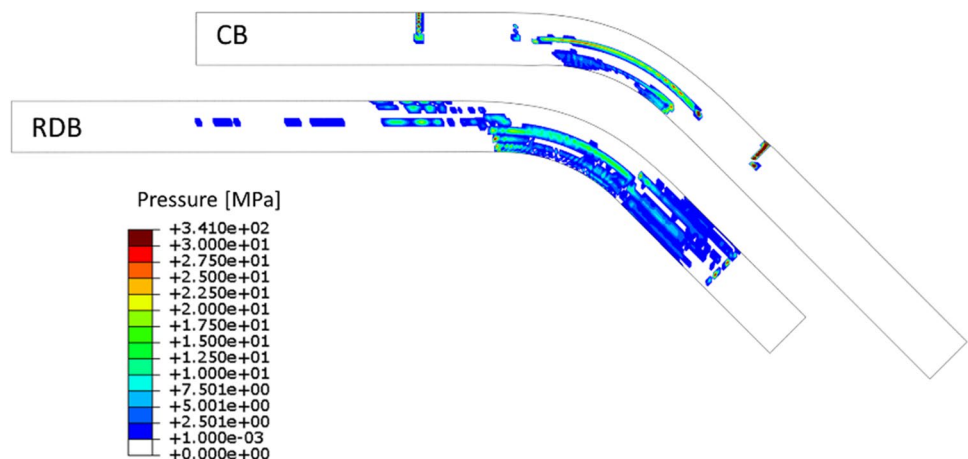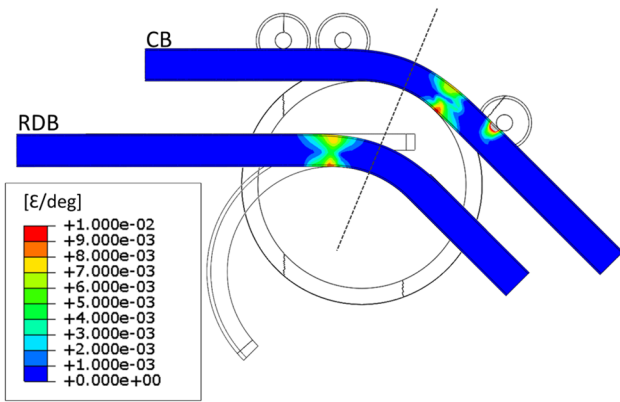
Fig. 15 Bend angle derivative of plastic equivalent strain averaged over the range of 40 to 45 degrees ($\Delta\varepsilon_{peq}/\Delta\theta$). Dotted line marks identical position

by Li et al. [12]. The reason for the discrepancy could be a slight misalignment of tools, incapability of replicating the complex friction forces between the tube and tooling, numerical inaccuracies due to a large number of iterations, through-thickness variation of material properties due to,

say, surface recrystallization during extrusion, or tool stiffness, as found to be significant for wrinkling defects by Borchmann et al. [25].

As shown in the radial plots, both the maximum widening and compression occur around 25–30 degrees for CB, with a distinct peak at this position. This is in contrast with RDB, where the compression and widening are more uniformly distributed along the whole segment. As a note, prior research on RDB mostly measures the cross-sectional distortion at the mid angle, which is not representative of the max distortion for CB. This is especially true for cross-sectional widening in the direction of the bend axis, where the maximum is positioned at about 20–25 degrees into the bend for all investigated angles. For compression radial to the bend axis, the maximum values are positioned between 20 and 35 degrees into the bend.

Figure 18 shows that the deformation of the cross section is dominated by the changes in the outer part of the tube's cross section for both processes, creating a D-shape with a somewhat flattened extrados. This flattened region is significantly wider for CB than for RDB. It also exhibits a tighter radius at the ends of this flat region, meeting up with the nearly unchanged intrados. As seen in Fig. 19,

Fig. 16 Radial plot of tube cross-sectional compression (flattening) from nominal diameter, radial to bend axis for RDB and CB specimens together with finite element results after release. Opaque region shows the results spread for the two samples. Final angle (86.1°) is the average angle for all four samples
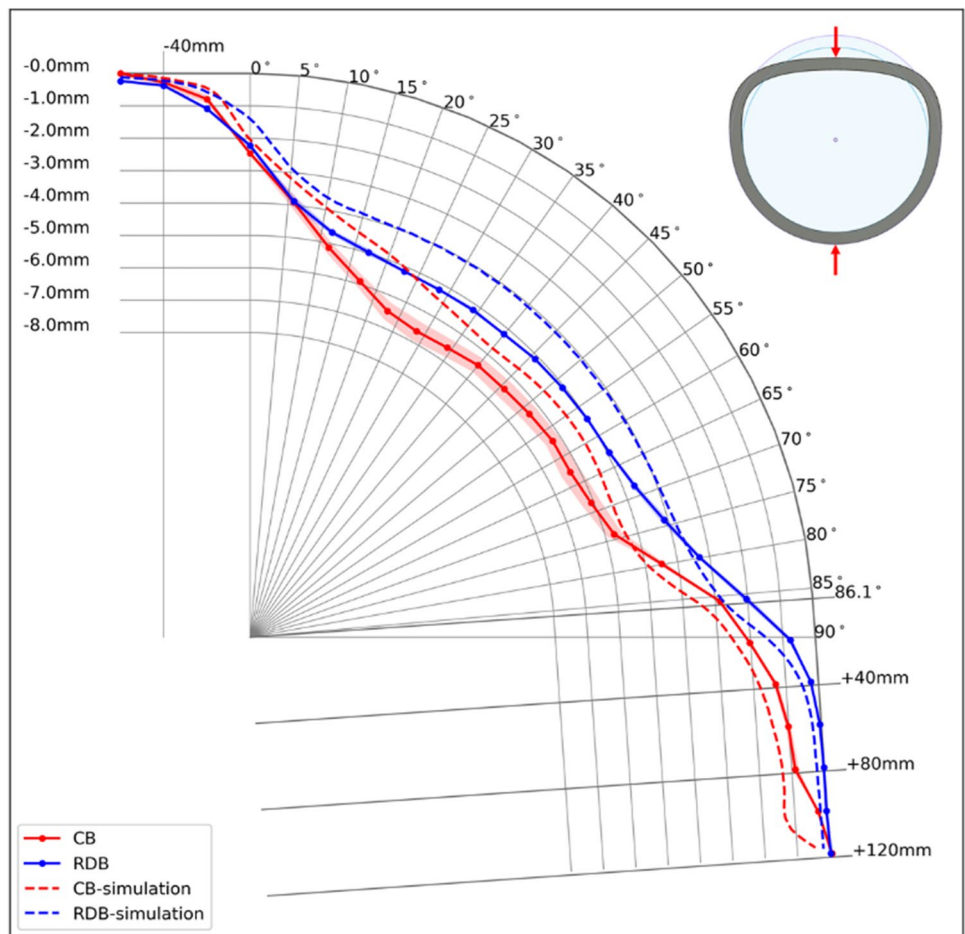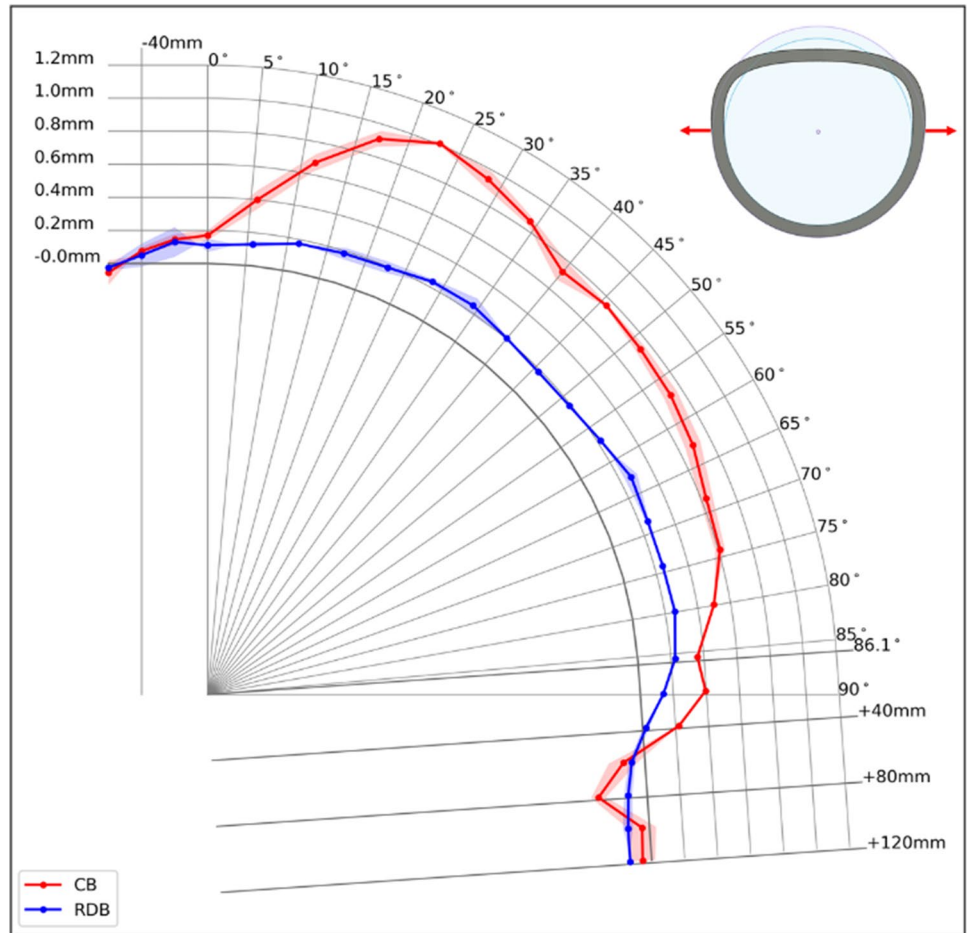
Fig. 17 Radial plot of tube cross-sectional widening along bend axis from the 60 mm nominal diameter together with finite element results after release. Opaque region shows the results spread for the two samples per process. Final angle (86.1°) is the average angle for all four test samples

the cross section of both RDB and CB starts to diverge from the nominal circular shape below the center line of the bend, despite the fact that this section is supported by the bend die during the process. This indicates that there is some elastic relaxation, or springback, in the direction of the bend axis, after the tube portion has been bent, either during the process or after release. An alternative explanation is that the tube portion being bent does not reach the bottom of the tool grove during plastic deformation. The contact pressure values in Fig. 13 and the strain evolution

in Fig. 15 suggests that the first would most likely be the case, as there seems to be contact at the bend die at the positions of yielding both for RDB and CB.

Figure 20 displays the shear stress (in-plane longitudinal/transverse direction, $\sigma_{z\theta}$, in local directions) for both processes. As hypothesized above, there is a slight increase in shear stress for RDB, and a more sustained region of high shear stress between the pressure die and bend die. This is in contrast to CB, which provides a lower and more discontinuous field between forming roller and bend die.
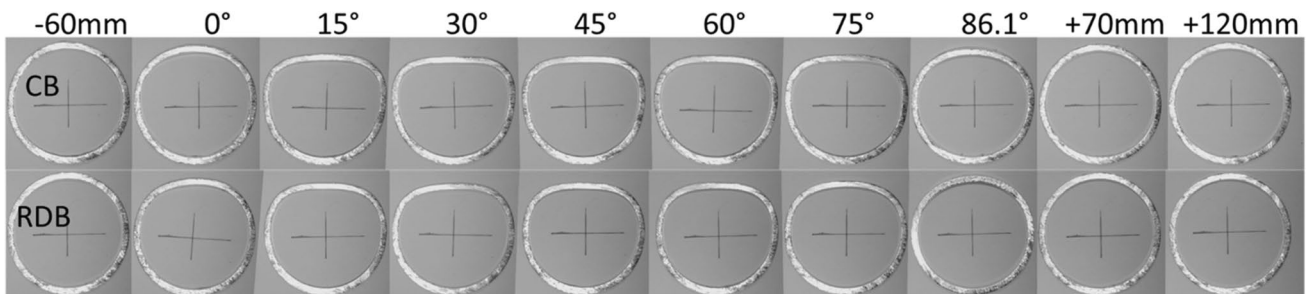
Fig. 18 Cross section evolution along nominal 90-degree bend, with an average resultant angle of 86.1. Extrados is aligned upwards
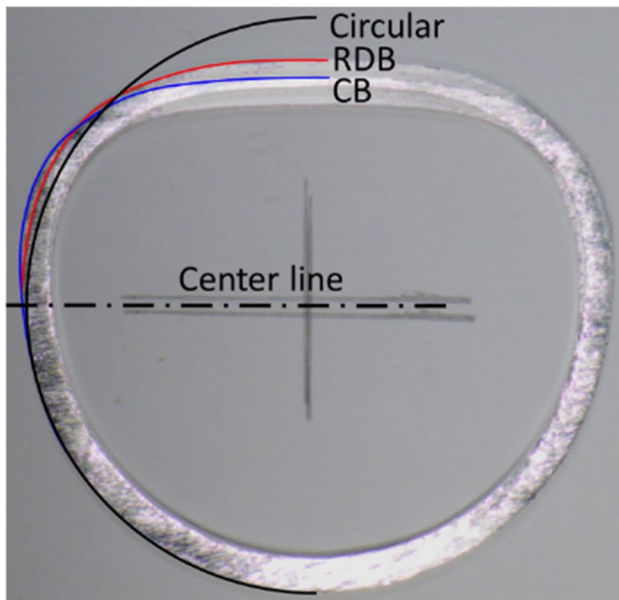
Fig. 19 Overlay of RDB over CB image at 45 degree angle for 90 degree specimens, with outer maxima traced for improved visibility. Half circle added for reference. Circular curve and center line fitted to intrados curve

This would increase the shear deformations for RDB, but as the results show, other factors seem to drive the majority of the deformations, as CB exhibits larger deformations in general. The difference between RDB and CB regarding cross sectional compression is minor in the range where the forming roller does not have contact with the tube, while almost uniformly 1–1.5 mm in the range where the forming
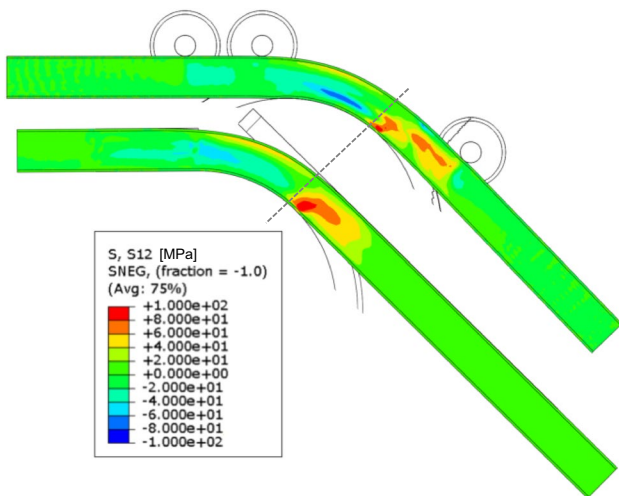
Fig. 20 In-shell shear stress (longitudinal/transverse direction) for CB and RDB for position at 45 degrees during bending. The RDB image is (in this figure only) mirrored, angled and values inversed to easier compare the two processes. Dotted line mark similar positions

roller interacts. We believe the majority of the increased compression (as seen in Fig. 16) for CB is caused by the heightened contact pressure of the forming roller, compared with that of the pressure die, but it would also be affected by the lack of initial moment caused by the clamp die for RDB.

3.3 Change in wall thickness

As displayed in Fig. 21, there is a slight difference between RDB and CB regarding intrados thickening, with approximately 0.03–0.09 mm larger intrados thickening trend, with a maximum of 0.36 mm wall thickness increase for CB compared to 0.30 for RDB. Maximum extrados thinning is similar for the processes, with 0.19 mm wall thickness decrease maximum, but the trend is larger for RDB with about 0.03–0.07 mm.

As a note on FEA accuracy, the FEA results predicted a similar intrados thickening, close to the experimental results (0.34 mm and 0.31 mm maximum for CB and RDB respectively), but a larger difference in the extrados thinning, trending at 0.1–0.15 mm more thinning for RDB, while having the same maximum levels (0.25 mm). The CB simulation agrees well with the experimental results, while the RDB simulation overestimates the extrados thinning. This is somewhat expected, as the FEA results for RDB underestimated the compression of the cross section, and hence would have increased strain levels in general, but the difference seems so large that some other effects might also be contributing to this underestimation.

Much of this difference between RDB and CB is assumed to be caused by a difference in the bending strain neutral layer shift, which is also seen in the numerical results, as displayed in Fig. 22. Based on the FEA results, the position for the neutral layer for CB has a 3.5 mm inward shift at 45 degrees measured from the intrados in the numerical results, while RDB displays a 5.5 mm inward shift (2 mm difference). If measuring from the center line of the compressed tube, the inward layer shift becomes 0.6 mm and 3.9 mm (3.3 mm difference) for CB and RDB, respectively, due to the difference in compression of the cross section. The reason for the observed neutral layer shift is not clear but could potentially be related to differences in how the cross section deforms locally, the additional moment caused by the clamp die for RDB, and/or differences in external traction introduced by friction.

Although minor, the difference in wall thickness could potentially have a considerable effect on thickness sensitive phenomenons, e.g., buckling behavior. For a cubic relationship, the reduction in wall stiffness per unit length from a 2.9 mm to a 2.81 mm thick planar wall would be

Fig. 21 Measured difference of extrados and intrados wall thickness compared with the thickness measured at the ends of the tube, at respective positions for RDB and CB along tube bend. Final angle (86.1°) is the average angle for all four samples
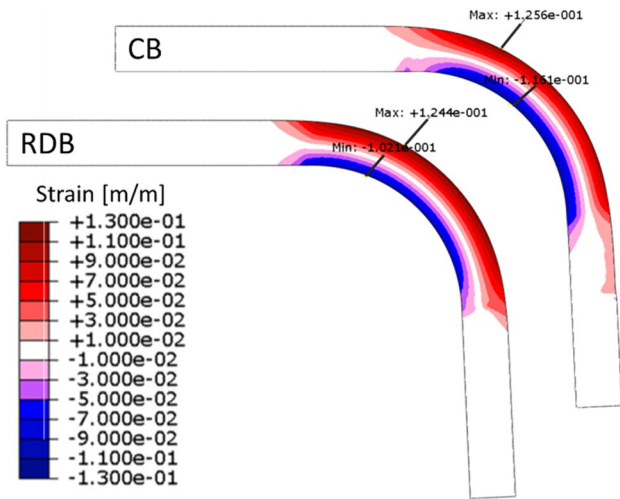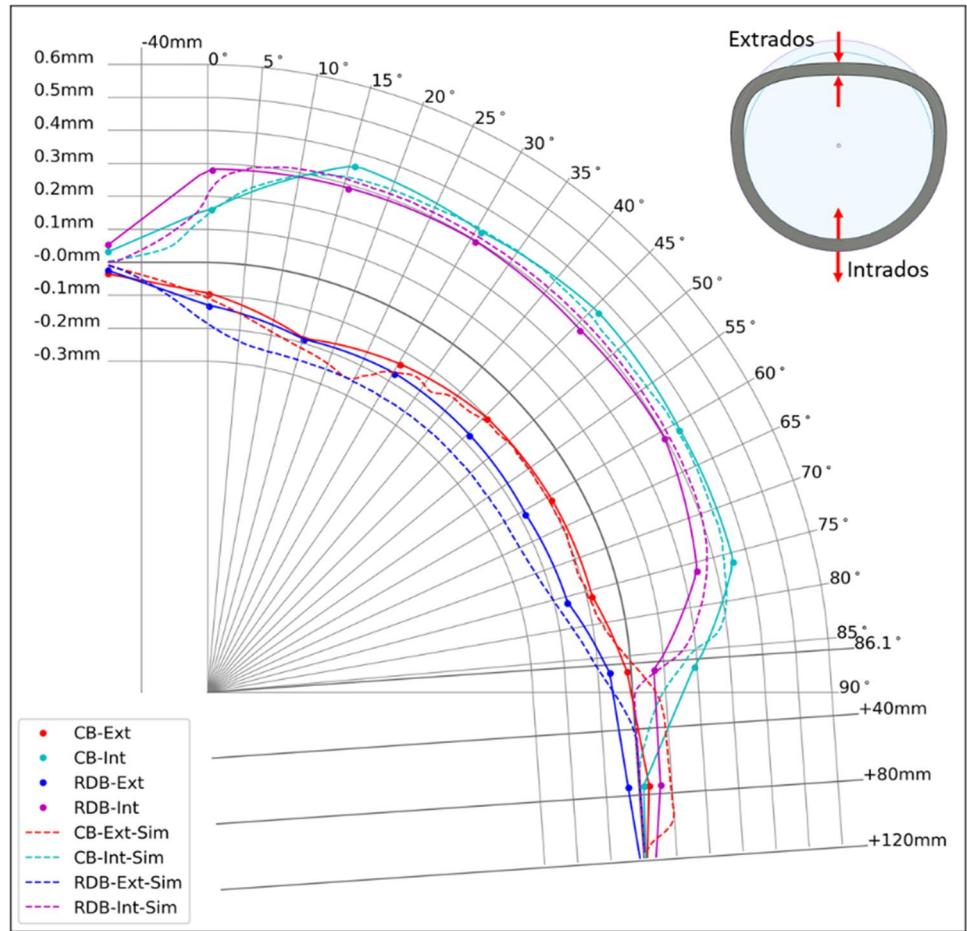

Fig. 22 Plastic strain in longitudinal direction for CB and RDB after release, displaying a similarly matched extrados strain (0.124 for RDB vs 0.126 for CB) and a larger difference on the intrados strain (−0.116 for CB vs. −0.102 for RDB). Neutral layer for plastic strain shifted 3.4 mm towards intrados for CB, while 5.7 mm for RDB measured from tool center

approximately 9%. It must be noted that this difference in thickening/thinning is less than the wall thickness accuracy (± 0.25 mm according to ISO EN-755–9:2016 for the given size and alloy). The dimensions of the tube blanks could therefore be of more importance than the bending method.

4 Conclusions and key takeaways

Although often considered an inferior process to rotary draw bending, this investigation has shown that (roller based) compression bending could be a viable alternative to mandrel-less rotary draw bending.

In the case of bending 60 × 3 mm cross Sect. 6060-T4 aluminum alloy tubes around a bend die with a radius of 222 mm, both roller-based compression bending and rotational draw bending create a smooth bend with no significant wrinkles or local distortions, other than a slight bulge at the stop position of the forming roller for CB. The results show that both methods create springback to such an extent

that it would most often need to be compensated for, but it must be noted that the magnitude is slightly smaller for CB compared to RDB.

For applications relying on a tight fit with the extrados shape, it is noteworthy that the two processes produce different nominal extrados shapes. CB displays 0.89–1.76 mm larger cross-sectional flattening and 0.59–0.73 mm larger widening than for RDB, which is considerable. This implies that those applications requiring a tight fit to the extrados or sides of the tube would need to be redesigned for substituting RDB with CB. For mechanical performance, the increased flattening of the cross section would give a reduction in stiffness and load-carrying capacity for forces applied in the bend-plane of CB parts compared to RDB parts. The latter could be important for durability, e.g., fatigue behavior, of the final product.

The extrados wall thinning is, for the case considered, found to be somewhat higher for RDB (0.03–0.07 mm larger thinning), while the intrados thickening is found to be smaller by approximately the same magnitude (0.03–0.09 mm smaller thickening). This will be expected to create different elastic buckling resistances of the product due to its cubic relation with wall thickness, but as this is dependent on other factors—such as the deformation and curvature of the cross section—the full effect of this difference is not assessed. The difference is, however, less than usual manufacturing tolerances for extruded tubes in aluminum, and the dimensions of the tube blanks would therefore often be of equal or higher importance.

Within the scope of the cases investigated, this study shows that although there is a possibility of using TPRB tooling for CB as a substitute for RDB, there is some penalty in terms of sacrificed dimensional capability for doing so. Therefore, RDB would still be the first choice for tight-tolerance bending. However, in the case of lack of tooling for RDB, or configurations that need wide curves going directly into a sharp(er) bend, CB could provide that capability once geometric dimensions and tolerancing issues are carefully considered. Moreover, as TRPB with this functionality is very common in the industry, there may already be room for more widespread adoption of CB for low-cost applications.

Author contribution The individual contributions are as following: Tronvoll, S.A. has been involved in the conceptualization of the research, conducting experimental and numerical work, interpreting of data, and has been the main author of the paper, including writing first draft, Ma, J. has been assisting on conducting experimental and numerical work, interpreting of data, and revising the paper, Welo, T. has been involved in the conceptualization of the research, interpreting of data, and revising the paper. All authors have read and approved the final manuscript.

Declarations

Conflict of interest The authors declare no competing interests.

References

1. Kervick RK, Springborn RJ (1966) Cold bending and forming tube and other sections, 1st ed. Am Soc Tool Manuf Eng, Dearborn, Michigan. https://books.google.no/books?id=s7aWW-Jk9VgC&pg=PA72&source=gbs_toc_r&cad=3#v=onepage&q&f=false

2. Miller G (2003) Tube forming processes : a comprehensive guide. Society of Manufacturing Engineers, Dearborn, Michigan. https://openlibrary.org/books/OL5989127M/Cold_bending_and_forming_tube_and_other_sections

3. Ghiotti A, Simonetto E, Bruschi S, Bariani PF (2017) Springback measurement in three roll push bending process of hollow structural sections. CIRP Ann 66:289–292. https://doi.org/10.1016/j.cirp.2017.04.119

4. Simonetto E, Ghiotti A, Bruschi S (2017) Dynamic detection of tubes wrinkling in three roll push bending. Procedia Eng 207:2316–2321. https://doi.org/10.1016/j.proeng.2017.10.1001

5. He Y, Jing Y, Mei Z et al (2009) 3D numerical study on wrinkling characteristics in NC bending of aluminium alloy thin-walled tubes with large diameters under multi-die constraints. Comput Mater Sci 45:1052–1067. https://doi.org/10.1016/j.commatsci.2009.01.010

6. He Y, Lin Y (2004) Wrinkling analysis for forming limit of tube bending processes. J Mater Process Technol 152:363–369. https://doi.org/10.1016/j.jmatprotec.2004.04.410

7. Brazier LG, Southwell RV (1927) On the flexure of thin cylindrical shells and other "thin" sections. Proc R Soc Lond Ser Contain Pap Math Phys Character 116:104–114. https://doi.org/10.1098/rspa.1927.0125

8. Hill R (1950) The mathematical theory of plasticity. Oxford University Press, Oxford

9. Pan K, Stelson KA (1995) On the plastic deformation of tube during bending. J Eng Ind Trans ASME 117(4):494–500. https://doi.org/10.1115/1.2803526

10. Paulsen F, Welo T (2003) An analytical model for prediction of tube ovalization in bending. ESAFORM 2003 Proc Sixth ESAFORM Conf Mater Form 775–778

11. Safdarian R (2020) Investigation of tube fracture in the rotary draw bending process using experimental and numerical methods. Int J Mater Form 13:493–516. https://doi.org/10.1007/s12289-019-01484-5

12. Li H, Yang H, Zhan M, Kou YL (2010) Deformation behaviors of thin-walled tube in rotary draw bending under push assistant loading conditions. J Mater Process Technol 210:143–158. https://doi.org/10.1016/j.jmatprotec.2009.07.024

13. Yang H, Li H, Zhan M (2010) Friction role in bending behaviors of thin-walled tube in rotary-draw-bending under small bending radii. J Mater Process Technol 210:2273–2284. https://doi.org/10.1016/j.jmatprotec.2010.08.021

14. Dohda K, Yamamoto M, Hu C et al (2021) Galling phenomena in metal forming. Friction 9:665–685. https://doi.org/10.1007/s40544-020-0430-z

15. Kim H, Sung J, Goodwin FE, Altan T (2008) Investigation of galling in forming galvanized advanced high strength steels (AHSSs) using the twist compression test (TCT). J Mater Process Technol 205:459–468. https://doi.org/10.1016/j.jmatprotec.2007.11.281

16. Heng L, He Y, Mei Z et al (2007) Role of mandrel in NC precision bending process of thin-walled tube. Int J Mach Tools Manuf 47:1164–1175. https://doi.org/10.1016/j.ijmachtools.2006.09.001

17. Ma J, Ha T, Blindheim J et al (2020) Exploring the influence of pre/post-aging on springback in Al-Mg-Si alloy tube bending. Procedia Manuf 47:774–780. https://doi.org/10.1016/j.promfg.2020.04.239

18. Tekkaya AE, Chatti S (2014) Bending (Tubes, Profiles). In: Laperrière L, Reinhart G (eds) CIRP encyclopedia of production engineering. Springer, Berlin, pp 92–101

19. Borchmann L, Kuhnhen C, Frohn P, Engel B (2019) Sensitivity analysis of the rotary draw bending process as a database of digital equipping support. Procedia Manuf 29:592–599. https://doi.org/10.1016/j.promfg.2019.02.100

20. Kale AV, Thorat HT (2014) Control of ovality in pipe bending: a new approach. Proc 26th All India Manuf Technol Des Res Conf (AIMTDR 2014), Assam, India

21. Hydro Innvation and Technology Technical datasheet - Extruded products Alloy EN AW-6060 [AlMgSi]. https://www.hydro.com/Document/Index?name=Hydro%20EN%20AW%206060.PDF&id=7822. Accessed 12 Apr 2021

22. Hill R, Orowan E (1948) A theory of the yielding and plastic flow of anisotropic metals. Proc R Soc Lond Ser Math Phys Sci 193:281–297. https://doi.org/10.1098/rspa.1948.0045

23. Aretz H (2007) Numerical analysis of diffuse and localized necking in orthotropic sheet metals. Int J Plast 23:798–840. https://doi.org/10.1016/j.ijplas.2006.07.005

24. Kawka M, Makinouchi A (1996) Plastic anisotropy in FEM analysis using degenerated solid element. J Mater Process Technol 60:239–242. https://doi.org/10.1016/0924-0136(96)02336-9

25. Borchmann L, Heftrich C, Engel B (2020) Influence of the stiffness of machine axes on the formation of wrinkles during rotary draw bending. SN Appl Sci 2:1627. https://doi.org/10.1007/s42452-020-03419-1